14th International Symposium on Turbulence and Shear Flow Phenomena (TSFP14)
Heidelberg, Germany, July 28-31, 2026

DNS AND MODELING OF AN OSCILLATING TURBULENT BOUNDARY LAYER

Hiroyuki Abe
Japan Aerospace Exploration Agency
Chofu, Tokyo 182-8522, Japan
abe.hiroyuki@jaxa.jp

Philippe R. Spalart
Boeing Commercial Airplanes (Retired)
Seattle, Washington 98124, USA
prspalart@gmail.com

ABSTRACT

In the present study, we have performed a series of direct numerical simulations (DNSs) of an oscillating turbulent boundary layer (TBL) over a range of Reynolds numbers. The freestream velocity varies sinusoidally in time, leading to adverse and favorable pressure gradients. Three values of the Reynolds number ($Re_{\delta s}$ =1000, 1400 and 1800) are used, where $Re_{\delta s}$ is based on the freestream velocity and travel, and the laminar boundary-layer thickness. Particular attention is given to the effects of the Reynolds number together with those of the mean pressure gradient (for the inner-normalized pressure gradient range $p^+ \approx$ -0.02 to 0.02) on the mean and second-order moments. Their inspection reveals a similarity in the U^+-versus-y^+ profile between the present flow and other wall-bounded flows (i.e., channel and spatially-evolving TBLs) at least for a moderate value of p^+. The functional dependence on p^+ for the mean velocity and the active second-order moments is also clarified. Also presented is an evaluation of Reynolds-averaged Navier-Stokes equation (RANS) turbulence models such as SA, SST and k-ε using the present DNS data.

INTRODUCTION

The effects of the pressure gradient on wall-bounded turbulent flows have attracted significant attention over many decades. The adverse-pressure gradient (APG) retards a TBL and may eventually lead to separation, whereas the strong favorable-pressure gradient (FPG) can yield reminaralization. Their understanding and prediction are however still not satisfactory, especially for a flow with rapidly-varying pressure gradient either in space or, like here, in time.

Here, the flow under consideration is a turbulent version of the Stokes second problem (Schlichting and Gersten 2000). The freestream flow is an oscillating flow with sinusoidal variation in time, while the wall is a stationary smooth flat plate. The freestream velocity is given by

$$U_\infty = U_0 \cos(\omega t) \quad , \qquad (1)$$

where U_0, ω and t denote the peak value of freestream velocity, frequency, and time. The mean pressure gradient is the time-derivative of the velocity and therefore also varies sinusoidally in time. One half-cycle consists of the phase-angle φ=ωt=0 to π and it is repeated in reverse. In the cycle, the APG is first imposed (φ=0 to π/2), causing a reversal of the wall shear stress equivalent to separation in a spatially-developing flow. The FPG is subsequently imposed ($\varphi = \pi/2$ to π) so that the flow which has reversed direction is attached and then momentarily exhibits a laminar-like velocity profile, if the Reynolds number is low enough. As the FPG weakens, the flow again approaches the zero-pressure-gradient TBL (for φ =0 and π).

The seminal DNS study was performed by Spalart and Baldwin (1989) at $Re_{\delta s}$ = 600 to 1200. Their Reynolds numbers include the transitional Re range, which is unusually difficult for RANS models. In the current DNS, higher values of the Reynolds number ($Re_{\delta s}$ =1000, 1400 and 1800) are used to compare with the measurements of Jensen et al. (1989). The latter two Reynolds numbers are close to being free of low-Re effects. The objectives of the present study are to clarify the effects of the Reynolds number and the pressure gradient on turbulence statistics and structures, and also to establish the possible functional dependence of the mean and second-order moments.

Attention is also given to the evaluation of RANS turbulence models (e.g., SA (Spalart-Allmaras 1994), SST (Menter 1994) and k-ε (Abe et al. 2023)) using the DNS data. It is hoped that, although the response to the pressure gradient is different among the models, the present testing may provide further insight into how the current models respond to varying pressure gradients and provide predictions for both the APG and FPG regions.

NUMERICAL METHDOLOGY

The computational domain is given in Fig. 1 where x, y and z refer to the streamwise, wall-normal and spanwise directions, respectively. The present flow is incompressible. The governing equations consist of the continuity equation

$$\frac{\partial U_i}{\partial x_i} = 0 \qquad (2)$$

and the Navier-Stokes momentum equations

$$\frac{\partial U_i}{\partial t} + U_j \frac{\partial U_i}{\partial x_j} = -\frac{1}{\rho}\frac{\partial P}{\partial x_i} + \nu \frac{\partial^2 U_i}{\partial x_j^2} - \frac{\partial \overline{P}}{\partial x_1}\delta_{i1} \qquad (3)$$

Note that U_1, U_2, U_3 denote the instantaneous streamwise, wall-normal, and spanwise velocities, respectively; U, V, W are also used interchangeably with U_1, U_2, U_3 across the paper; an overbar represents an average with respect to space in the homogeneous directions (i.e. the x and z directions) at a fixed phase angle φ. ρ and ν refer to the density and viscosity. The DNSs are performed with doubly-periodic boundary conditions in the x and z directions while the mean pressure gradient varies sinusoidally in time, being given by

$$p \equiv \frac{1}{\rho}\frac{\partial \overline{P}}{\partial x} = -\frac{\partial U_\infty}{\partial t} = U_0 \omega \sin(\omega t). \qquad (4)$$

Eq. (4) reproduces the freestream variation of the oscillating flow as noted in Eq. (1).

The numerical methodology is briefly as follows. The current DNS code has been developed based on the boundary layer DNS code (Abe 2020). A fractional step method is used with semi-implicit time advancement. The Crank-Nicolson method is used for the viscous terms in the y direction, and the 3rd-order Runge-Kutta method is used for

Table 1. Domain size, grid points and spatial resolution.

$Re_{\delta s}$	1000	1400	1800
Re_a	5.0×10^5	9.8×10^5	1.62×10^6
$L_x\times L_y\times L_z$	$0.4a\times0.2a\times0.2a$	$0.4a\times0.2a\times0.2a$	$0.4a\times0.2a\times0.2a$
$N_x\times N_y\times N_z$	$1024\times384\times1024$	$2048\times512\times2048$	$3072\times768\times3072$
Δx^+, Δy^+, Δz^+	10.0, 0.13 – 19.3, 5.02	9.03, 0.13 – 27.2, 4.51	9.61, 0.13 – 29.4, 4.81

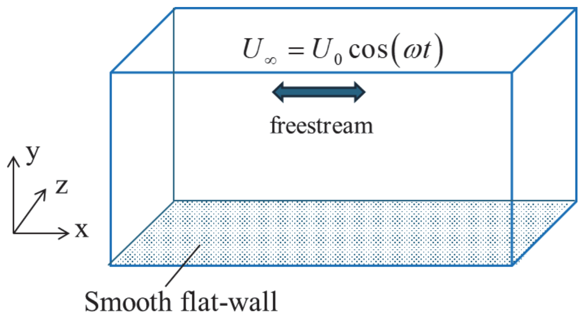

Figure 1. Computational domain.

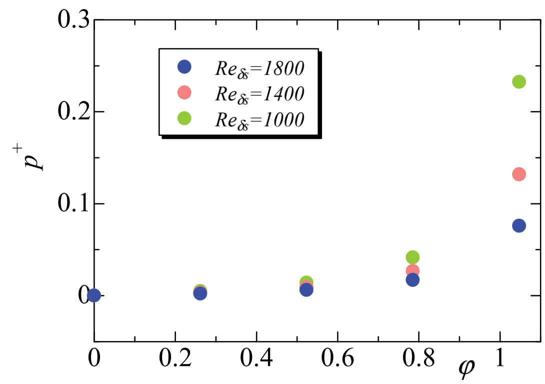

Figure 3. Distributions of p^+ for the APG phase.

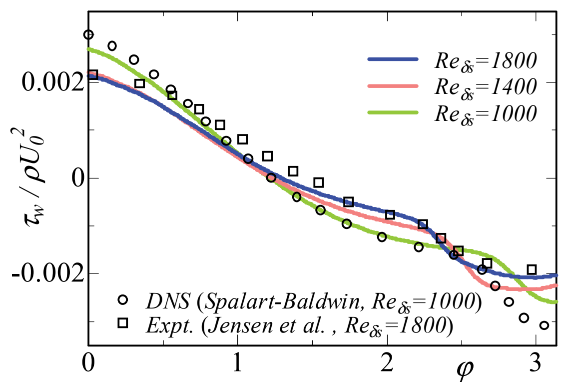

Figure 2. Skin friction.

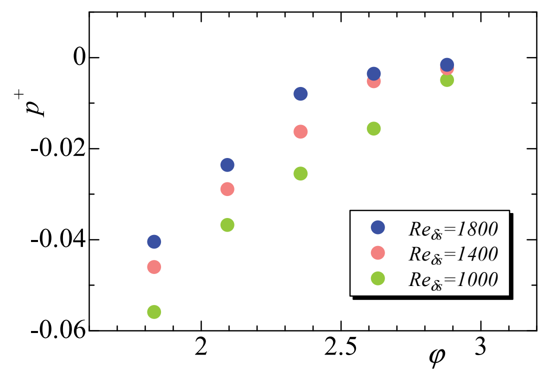

Figure 4. Distributions of p^+ for the FPG phase.

the other terms. A finite difference method is used as a spatial discretization. A 4th-order central scheme (Morinishi et al. 1998) is used in the x and z directions, whilst a 2nd-order central scheme is used in the y direction. The computational domain size ($L_x\times L_y\times L_z$), number of grid points ($N_x\times N_y\times N_z$) and spatial resolution (Δx^+, Δy^+, Δz^+) are given in Table 1 where the superscript + denotes normalization by wall units (the friction velocity U_τ and the viscous length scale ν/U_τ); Re_a the Reynolds number based on $a=U_0/\omega$; Δy^+ refers to the spatial resolution at the wall and that at $y/a=0.05$ where the mean velocity is almost identical with Eq. (1). The present study uses a relatively large spanwise domain to properly accommodate large-scale structures of streamwise velocity fluctuations when the APG is imposed (see Fig. 8b). Another motivation is to enlarge the statistical sample. The number of half-cycles used for the phase-averaging is approximately 6, 4 and 4 for $Re_{\delta s}$ =1000, 1400 and 1800, respectively. Also note that the number of points in each direction essentially scales with the square of the Reynolds number so that the largest number of grid points is 7.2 billion to resolve the essential motions of turbulence at $Re_{\delta s}$ =1800.

RESULTS AND DISCUSSION

We first discuss the friction coefficient $\tau_w / \rho U_0^2$. Figure 2 shows the normalized profile during one half-cycle (φ = 0 to π) for the three Reynolds numbers $Re_{\delta s}$ =1000, 1400 and 1800. The current data are compared with the DNS result of Spalart and Baldwin (1989) at $Re_{\delta s}$=1000 and the experimental one of Jensen et al. (1989) at $Re_{\delta s}$=1800; the agreement is good over a wide range of φ. The peak value decreases slowly with increasing Re. Separation occurs due to a large APG when the phase angle φ>1.2 ($Re_{\delta s}$ =1000) and φ >1.3 ($Re_{\delta s}$ =1400 and 1800). The curves show partial relaminarization under acceleration (FPG, φ ≈2), which will be discussed with the mean velocity. At $Re_{\delta s}$ =1000, there appears a large peak in the profile near φ =π. The two DNS studies exhibit significant differences. By contrast, the latter peak becomes moderate for $Re_{\delta s}$ =1400 and 1800; the profile varies slowly with $Re_{\delta s}$. The latter results indicate that two Reynolds numbers are essentially free of low-Re effects.

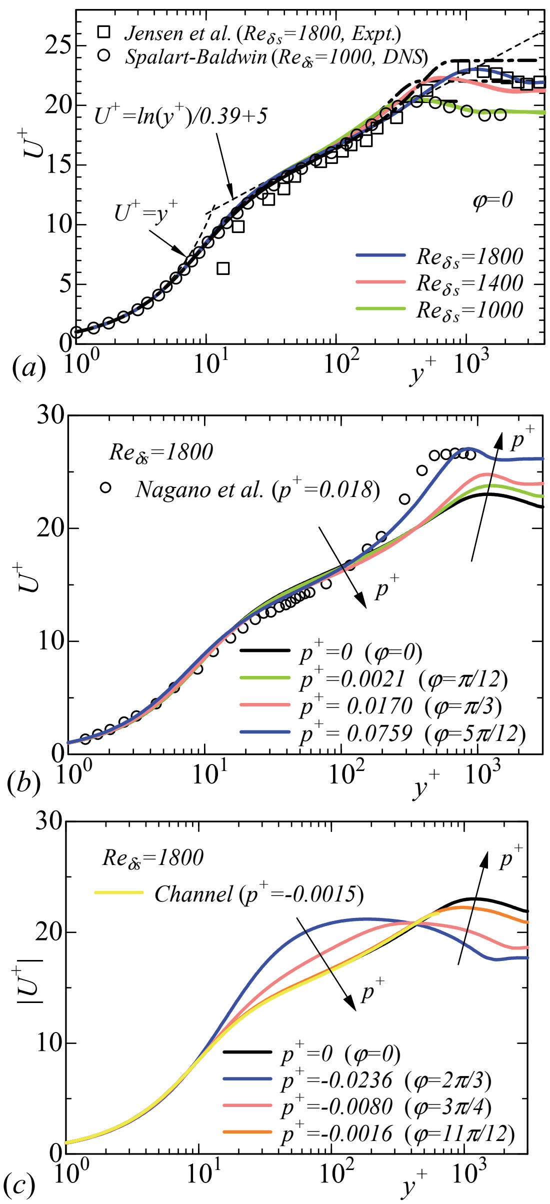

Figure 5. Distributions of U: (*a*) $Re_{\delta s}$ =1000, 1400, 1800 with φ=0; (*b*) $Re_{\delta s}$ =1800 (APG); (*c*) $Re_{\delta s}$ =1800 (FPG).

Figures 3 and 4 show the distributions of the inner-normalized mean pressure gradient, i.e.

$$p^+ = \frac{\nu}{\rho U_\tau^3} p \quad , \tag{5}$$

for the decelerating (APG) and accelerating (FPG) phases, respectively. For the APG phase, the magnitude of p^+ increases monotonically with the phase angle φ. The Reynolds-number dependence is larger for a larger φ. For the FPG phase, the magnitude decreases significantly with increasing Reynolds number at a fixed phase angle φ. At φ = 2 where the wall shear stress shows near a plateau, the largest magnitude of p^+ (=-0.0236) is attained at $Re_{\delta s}$=1800, which is consistent with the relaminarization condition p^+ =-0.018 of Patel (1968).

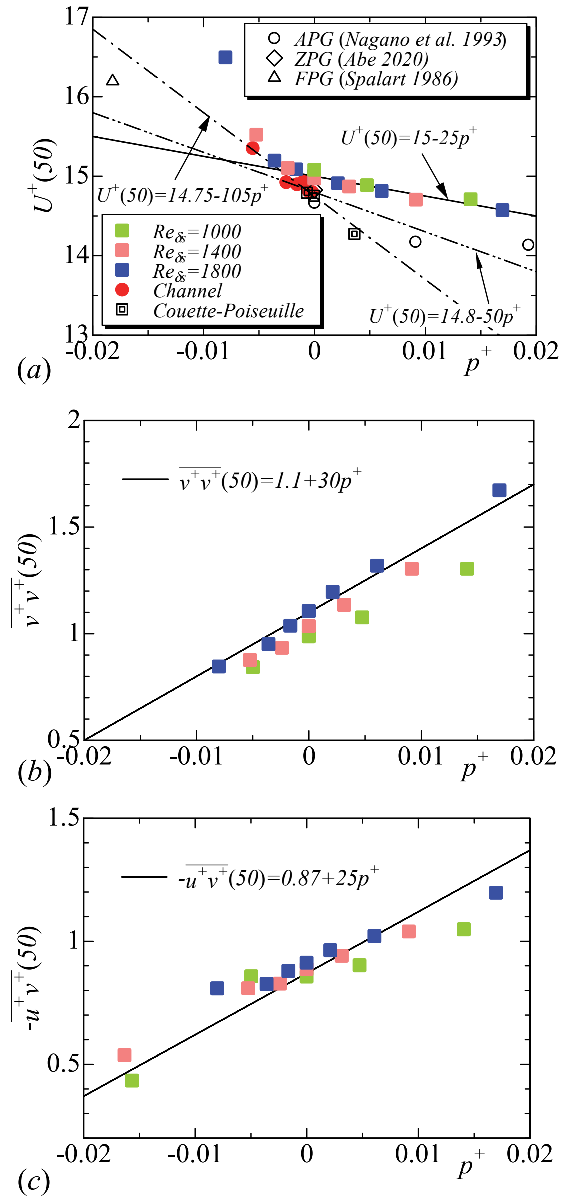

Figure 6. Distributions of U^+, $\overline{v^+v^+}$ and $-\overline{u^+v^+}$ at y^+=50 as a function of p^+ : (*a*) U^+, (*b*) $\overline{v^+v^+}$; (*c*) $-\overline{u^+v^+}$.

The normalized mean velocity profiles U^+ at the phase angle φ=0 are shown in Fig. 5a for $Re_{\delta s}$=1000, 1400 and 1800. The agreement with the DNS data of Spalart and Baldwin (1989) at $Re_{\delta s}$ =1000 and the experimental data of Jensen et al. (1989) at $Re_{\delta s}$ =1800 is satisfactory. We note that U^+ exhibits a good similarity to that in a zero-pressure gradient TBL when φ is close to 0: the U^+ profiles for $Re_{\delta s}$ =1000, 1400 and 1800 agree with the DNS data of the zero-pressure gradient (ZPG) TBL by Spalart (1988) at Re_θ =670, by Abe (2000) at Re_θ =1000, by Schlatter and Örlü (2009) at Re_θ =2000 (plotted as black lines).

Figures 5b and c show the U^+ profiles for $Re_{\delta s}$=1800 at several phase angles. In the APG phase (φ=0 to π/2), we see a logarithmic velocity profile over a wide range of φ. In the buffer and log regions, the magnitude of U^+ becomes slightly smaller with increasing φ and thus p^+. In contrast, when the

APG becomes strong, a large positive wake appears in the mean velocity profile. The current wake profile for $p^+ \approx 0.02$ however shows a smaller wake than with that of the APG TBL by Nagano et al. (1993) with nearly the same p^+. With this regard, a larger p^+ (≈ 0.08) in the present flow leads to nearly the same mean velocity profile, possibly indicating a difference in the history effects, but there is also the effect of a positive wall-normal velocity, present in only the spatially-developing flow, which effect is stronger in the outer layer. In the FPG phase ($\varphi=\pi/2$ to π), the magnitude of $|U^+|$ also becomes smaller with increasing p^+. The profile for $p^+=-0.0236$ displays a laminarized behavior, while that for $p^+=-0.0016$ agrees reasonably well with U^+ for the channel flow with nearly the same p^+ ($p^+=-0.0015$) where $p^+=-1/Re_\tau$ (Re_τ denotes the friction Reynolds number). These results indicate a similarity in the U^+ profile between the present flow and other wall-bounded flows (i.e., channel and spatially-evolving TBLs) at least in the very-near-wall region.

Here, we discuss the resilience of the law of the wall to varying p^+ and analyze the behaviors of the normalized mean velocity and Reynolds stresses at $y^+=50$ as a function of p^+ (Fig. 6). In this context, Johnstone et al. (2010) reported the p^+ dependence of U^+ in the logarithmic region of the APG TBL, in Couette-Poiseuille flow. The present DNS result supports their findings and highlights that U^+ decreases linearly with increasing p^+, although the behavior is less clear in a FPG (Fig. 6a where the existing channel (Abe et al. 2004*b*, 2009; Hoyas and Jimenez 2008; Lee and Moser 2015), Couette-Poiseuille (Johnstone et al. 2010) and TBL data (Spalart 1986; Nagano et al. 1993; Abe 2020) are also plotted). We note that the data for the current flow follows $U^+(50)=15-25p^+$, while those for the channel and Couette-Poiseuille flows follow $U^+(50)=14.8-50p^+$ and $U^+(50)=14.75-105p^+$ as proposed by Spalart and Abe (2021) and Johnstone et al. (2010), respectively. The reason for the difference in the p^+ slope could be due to the difference between internal and external flows. Given $p \equiv d\tau/dy$ and $d\tau/dy \approx -1/2\delta$ (τ and δ denote the total shear stress and boundary layer thickness, respectively) in the TBL flow (see also Spalart and Abe 2021), $p^+ = -1/2Re_\tau$ would hold in a 2D channel. The present slope for the linear dependence is therefore $1/Re_\tau = 50$, which is identical with that in an Inverse Re dependence of U^+ in canonical wall flows proposed by Luchini (2019) and Spalart and Abe (2021). At this y^+ location, the Reynolds stresses associated with the active motions ($\overline{v^+v^+}$ and $-\overline{u^+v^+}$) also exhibit linear variations but with a positive slope versus p^+ (Figs. 6b and c). This highlights a functional dependence on p^+ for the mean velocity and the active second-order moments in TBLs with pressure gradients. The notable fact is the weak dependence on Re, and the slope of 25 in the $-\overline{u^+v^+}$ value, which implies essentially no dependence for dU^+/dy^+; this fact can be deduced from the total shear stress. The same trend is observed at $y^+=100$ but with the slope of only about 50 (not shown here).

To gain further insights into the decreasing magnitude of U^+ in the buffer and log regions of the APG phase, we integrate the total shear stress τ up to $y^+=50$, i.e.

$$\int_0^{50} \frac{dU^+}{dy^+} dy^+ = \int_0^{50} \left(1 + p^+ y^+ + \overline{u^+v^+}\right) dy^+ \quad . \tag{6}$$

The LHS of Eq. (6) leads to $U^+(50)$, which we have seen is expressed as $U^+(50)=15-25p^+$ (see Fig. 6a). On the other hand, the RHS of Eq.(6) becomes

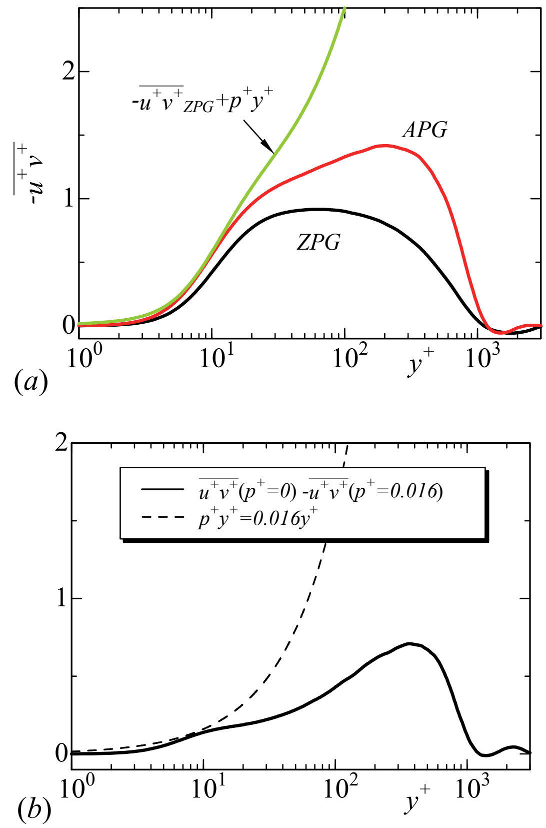

Figure 7. Distributions of $-\overline{u^+v^+}$ at $Re_{\delta s}$ =1800 in the ZPG (p=0) and APG (p^+=0.016) phases: (*a*) $-\overline{u^+v^+}$; (*b*) $\overline{u^+v^+}_{p^+=0} - \overline{u^+v^+}_{p^+=0.016}$.

$$RHS = \left[\frac{p^+ y^{+2}}{2}\right]_0^{50} - \int_0^{50}\left(-\overline{u^+v^+} - 1\right)dy^+ \tag{7}$$
$$= 1250\,p^+ - \int_0^{50}\left(-\overline{u^+v^+} - 1\right)dy^+$$

Given the magnitude of p^+ considered in the present study is $O(10^{-2})$, the decreasing magnitude of U^+ with increasing p^+ is due to how the change in the integral of $-\overline{u^+v^+}-1$ more than offsets the p^+ term. Figure 7a shows the distribution of $\overline{u^+v^+}$ in the ZPG (p^+=0) and APG (p^+=0.016) phases. Also, plotted in Fig. 7a is the distribution of the $p^+y^+ + \overline{u^+v^+}_{ZPG}$ term when p^+=0.01. The latter term (the green line) follows the $\overline{u^+v^+}$ profile in the APG phase. Figure 7b shows the distribution of $\overline{u^+v^+}_{p^+=0} - \overline{u^+v^+}_{p^+=0.016}$, which agrees reasonably with the p^+y^+ term. These results highlight that the effect of pressure gradient is associated with the difference in the integral of $-\overline{u^+v^+}$ between the APG and ZPG TBLs in the buffer layer and lower log regions. Another way to describe this is that the eddy viscosity responds significantly to pressure gradient, to the point that the total shear stress τ and the velocity shear rate $\partial U/\partial y$ change in opposite directions (Johnstone et al. 2010).

We also investigate the variation of the instantaneous fields in response to p^+ briefly. Figure 8 shows isosurfaces of the streamwise velocity fluctuations u at $Re_{\delta s}$ =1800 for φ = 0.1 (near ZPG) and 0.9 (APG). The visualized domain is the whole computational domain. When the phase angle is close

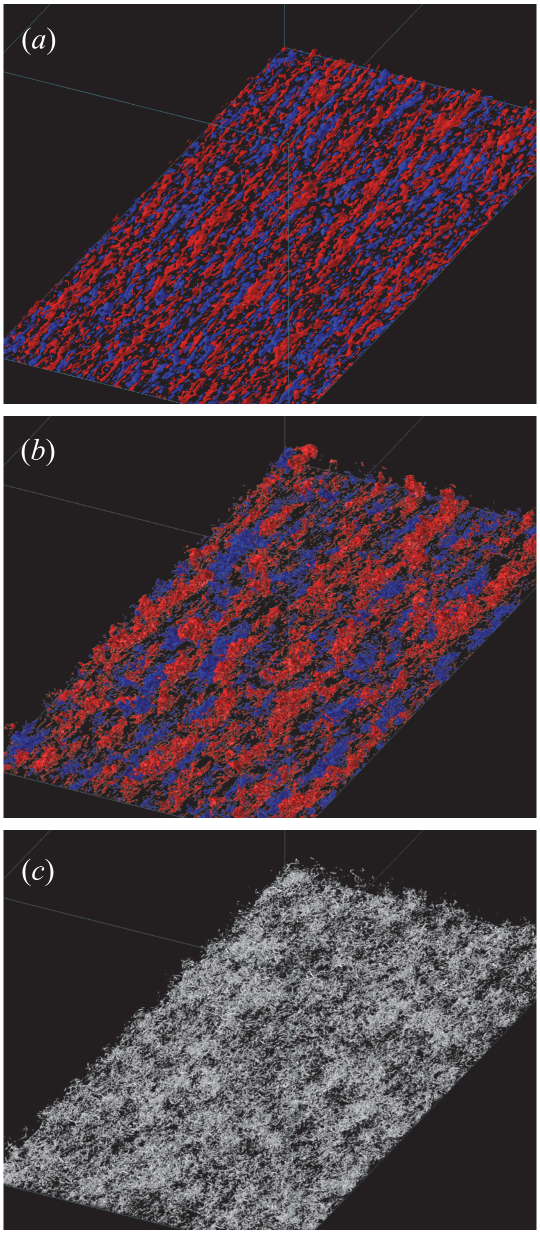

Figure 8. Isosurfaces of u and Q at $Re_{\delta s}$ =1800: (*a*) u (φ=0.1); (*b*) u (φ=0.9); (c) Q (φ=0.9). (a), (b) Blue, u>0.12; Red, u<-0.12; (*c*) white, Q>0.01. The fluid flows from bottom-left to top-right. Normalization is made with U_0 and a .

to 0, the magnitude of the mean-pressure gradient p^+ is small so that we see well-known streaky structures near a wall. At this Reynolds number, the streaky structures become densely clustered as was seen in the channel flow at a higher Re_τ (see, for example, Abe et al. 2004*a*). On the other hand, when the APG becomes large, the large-scale motions become prominent in the outer region, as was observed in the APG TBL (Lee and Sung 2009). Approximately 6 pairs of positive and negative large-scale u structures are observed in Fig. 8b, highlighting that the present spanwise domain is large enough to accommodate large scales even in the APG phase. The spanwise spacing is about 0.02 to 0.04a. Inspection revealed that the zero crossings of mean shear rate and Reynolds stress propagate away from the wall with the

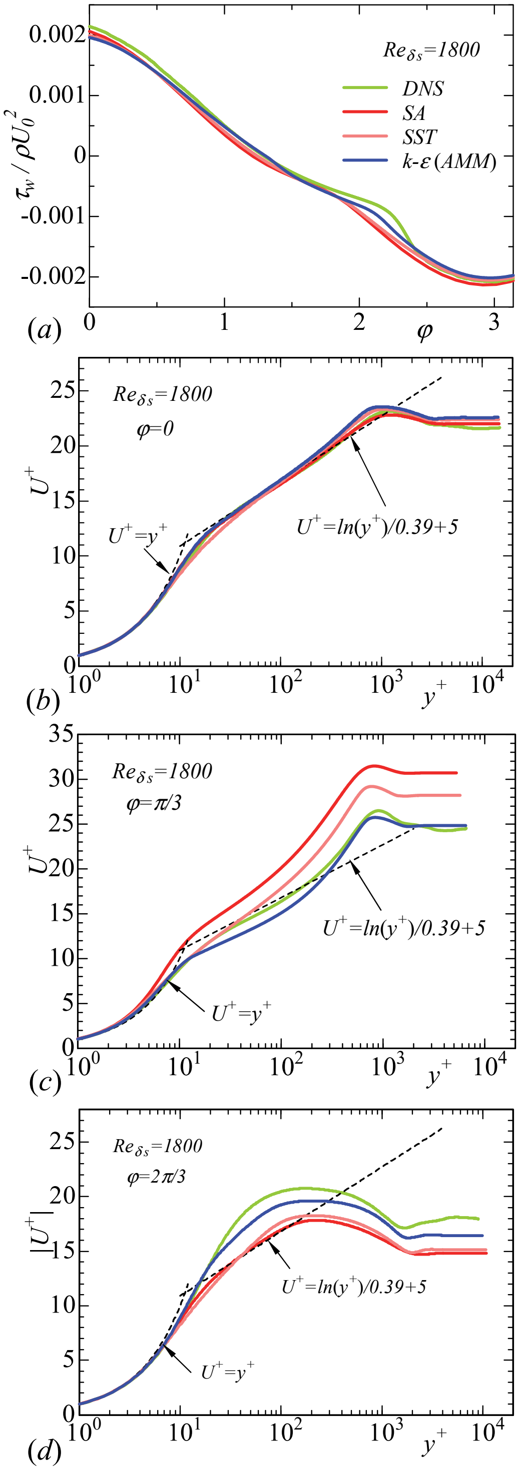

Figure 9. Predictions of the SA, SST and k-ε models at $Re_{\delta s}$ =1800; (*a*) τ_w; (*b*) U^+ (ZPG) ; (*c*) U^+ (strong APG); (*d*) U^+ (strong FPG).

convection velocity V≈0.012$a\omega$ for the three Reynolds numbers (not shown here). Since the propagation dominates in the outer region of the current flow, the boundary-layer thickness for φ=0 may be expressed as δ_0=V/ω ≈ 0.012a. The latter resulting value is consistent with the experimental result of Jensen et al. (1989) who obtained δ_0 based on the y location of the maximum U (see Fig. 24 of their paper and

Fig. 9 here). For the APG phase, the boundary-layer thickness is therefore $\delta = \delta_0 + V \approx 0.024a$. The normalized spanwise spacing is approximately δ to 2δ, which is close to that in the equilibrium APG TBL of Lee and Sung (2009). Figure 8c shows the isosurfaces of the positive Q (the second invariant of the velocity tensor) as a vortex indicator at $Re_{\delta s}$ =1800 for φ=0.9 (APG). Indeed, the vortical structures are energetic and show more tightly-clustered structures than the velocity, which is expected since Q is built from velocity derivatives. They are intrinsically associated with the large-scale structures of the streamwise velocity fluctuation.

Finally, we discuss the predictions of the RANS models for the present flow. In the calculations, the same grid is used as for the DNS in the y direction, which allows us to make direct comparisons between DNS and RANS results readily. Figure 9a shows the SA, SST and k-ε predictions for τ_w at $Re_{\delta s}$=1800. A noticeable difference appears between the DNS data and the model predictions for φ=2~2.5 (FPG), but otherwise the agreement is remarkably good. SA and SST change the distributions quickly compared to k-ε, which is essentially associated with the behavior that k-ε responds slowly to the varying pressure gradient. Consequently, for φ=0 (ZPG), k-ε overpredicts U^+; the U^+ prediction for SA is superior to that for k-ε (Fig. 9b), while the SST prediction is close to that of SA. On the other hand, for φ=π/3 (strong APG; $p^+\approx 0.08$), k-ε underpredicts U^+, while SA and SST overpredict U^+ (Fig. 9c). For 2π/3 (strong FPG; $p^+\approx$-0.02), all three models underpredict U^+ (Fig. 9d) and the relaminarized profile is simply missed. The present results indicate that the RANS models are not very accurate especially for large APG and FPG.

CONCLUSIONS

DNSs have been performed in an oscillating TBL over a wider range of Reynolds number than was achieved until now, namely up to $Re_{\delta s}$ =1800 versus 1000. The main conclusions are as follows.

1) τ_w for $Re_{\delta s}$ =1000 shows intense low-Re effects and a peak near φ =π which is not perfectly symmetric with that at φ=0, while that for $Re_{\delta s}$=1400 and 1800 varies predictably with increasing Re. Separation occurs due to a large APG approximately when φ >1.2 ($Re_{\delta s}$ =1000) and φ >1.3 ($Re_{\delta s}$ =1400 and 1800). Also, partial relaminarization is observed under acceleration near φ ≈2 for the three Reynolds numbers.
2) The present flow has a striking similarity to other wall-bounded flows (i.e., channel and spatially-evolving TBLs) as long as the PG is moderate.
3) In the buffer layer and lower log regions, there is a functional dependence on p^+ at a given y^+ for the mean velocity and the active second-order moments in TBLs with pressure gradients. This dependence on p^+ may be somewhat different between internal and external flows, or between temporally-evolving and spatially-evolving flows.
4) Inspection revealed that the (previously known) decrease of U^+ at a given y^+ in APG is essentially associated with the difference in the integral of $-\overline{u^+v^+}$ -1 between the ZPG and APG TBLs. This can be interpreted as a difference in eddy viscosity at a given y^+.
5) Like in the APG TBL, large-scale motions and vortex activity become prominent farther from the wall under APG.
6) The turbulence model testing reveals that the response to the varying pressure gradient is slightly slower in k-ε than in SA and SST. The latter models yield the best predictions when φ=0 whereas k-ε comes closest in terms of relaminarization. Generally, the RANS models are not as accurate for large APG and FPG, which is a common complaint.

REFERENCES

Abe, H., 2020, "Direct numerical simulation of a non-equilibrium three-dimensional turbulent boundary layer over a flat plate," J. Fluid Mech., Vol. 902, A20 (46 pages).

Abe, H., Antonia, R. A. and Kawamura, H., 2009, "Correlation between small-scale velocity and scalar fluctuations in a turbulent channel flow," J. Fluid Mech., Vol. 627, pp. 1-32.

Abe, H., Kawamura, H. and Choi, H., 2004*a*, "Very large-scale structures and their effects on the wall shear-stress fluctuations in a turbulent channel flow up to Re_τ = 640," Trans. ASME J. Fluids Engng, Vol. 126, pp. 835–843.

Abe, H., Kawamura, H. and Matsuo,Y., 2004*b*, "Surface heat-flux fluctuations in a turbulent channel flow up to Reτ = 1020 with Pr = 0.025 and 0.71, Int. J. Heat Fluid Flow, Vol. 25, pp. 404-419.

Abe, H., Nambu, T., Mizobuchi, Y. and Spalart, P.R., 2023, "Edge Behavior of the k-ε Model in Boundary Layers: Analysis and Improvement," AIAA Journal, Vol. 61, No. 12, pp. 5532-5547.

Jensen, B.L., Sumer, B.M. and Fredsoe, J., 1989, "Turbulent oscillatory boundary layers at high Reynolds number," J. Fluid Mech., Vol. 206, pp. 265−297.

Johnstone, R., Coleman, G. and Spalart, P.R., 2010, "The resilience of the logarithmic law to pressure gradients: evidence from direct numerical simulation," J. Fluid Mech., Vol. 643, pp. 163−175.

Hoyas, S. and Jiménez, J., 2008, "Reynolds number effects on the Reynolds-stress budgets in turbulent channels," Phys. Fluids, Vol. 20, 101511.

Lee, M. Lee and Moser, R. D., 2015, "Direct numerical simulation of turbulent channel flow up to Reτ ≈ 5200," J. Fluid Mech., Vol. 774, pp. 395–415.

Lee, J.-H. and Sung, H.J., 2009, "Structures in turbulent boundary layers subjected to adverse pressure gradients," J. Fluid Mech., Vol. 639, pp. 101-131.

Luchini, P., 2017, "Universality of the Turbulent Velocity Profile," Phys. Rev. Lett., Vol. 118, 224501.

Menter, F.R., 1994, "Two-equation eddy-viscosity turbulence models for engineering applications," AIAA J. 32 (8), pp. 1598–1605.

Morinishi, Y., Lund, T.S., Vasilyev, O.V. and Moin, P., 1998, "Fully Conservative Higher Order Finite Difference Schemes for Incompressible Flow," J. Comput. Phys., Vol. 143(1), pp. 90–124.

Nagano, Y., Tagawa, M. and Tsuji, T., 1993, "Effects of adverse pressure gradients on mean flows and turbulence statistics in a boundary layer," In: Durst, F., Friedrich, R., Launder, B.E., Schmidt, F.W., Schumann, U., Whitelaw, J.H. (eds) Turbulent Shear Flows 8, pp. 7–21, Springer.

Patel, V.C., 1965 "Calibration of the Preston tube and limitations on its use in pressure gradients," J. Fluid Mech. Vol. 23, pp. 185–208.

Schlatter, P. and Örlü, R., 2010 "Assessment of direct numerical simulation data of turbulent boundary layers," J. Fluid Mech., Vol. 659, pp. 116–126.

Schlichting, H. and Gersten, K., 2000, "Boundary Layer Theory," 8th revised and enlarged edition, pp. 129-130, Springer.

Spalart, P.R., 1986, "Numerical study of sink-flow boundary layers," J. Fluid Mech., Vol. 172, pp. 307–328.

Spalart, P.R., 1988, "Direct simulation of a turbulent boundary layer up to R_θ =1410," J. Fluid Mech., Vol. 187, pp. 61–98.

Spalart, P. R. and Abe, H., 2021, "Empirical scaling laws for wall-bounded turbulence deduced from direct numerical simulations," Phys. Rev. Fluids 6, 044604 (17 pages).

Spalart, P.R. and Allmaras, S.R., 1994, "A One-equation turbulence model for aerodynamic flows," La Rech. Aérospatiale, Vol. 1, pp. 5–21.

Spalart, P.R. and Baldwin, B.S., 1989, "Direct simulation of a turbulent oscillating boundary layer," Turbulent Shear Flows 6, pp. 417–440.

ACKNOWLEGDEMENTS

Computations performed on the JAXA Supercomputer System are gratefully acknowledged.